PHYSICAL REVIEW C **106**, 024604 (2022)

Statistical model calculation of the compound nuclear fission timescale in fusion-fission reactions

Rupinder Kaur,[1] Maninder Kaur,[1,*] and Santanu Pal[2,†]
[1] *Department of Physical Sciences, I.K.G. Punjab Technical University, Kapurthala -144603, India*
[2] *CS - 6/1, Golf Green, Kolkata -700095, India*

(Received 29 May 2022; accepted 26 July 2022; published 10 August 2022)

In the decay of an excited heavy nucleus, both the fission or evaporation residue (ER) cross sections and the fission time are determined by the competition between the various evaporation channels and fission. Statistical model (SM) calculations for several heavy-ion-induced fusion-fission reactions are presented which reproduce the fission or ER excitation functions. The corresponding calculated fission times are found to depend upon the compound nuclei and their excitation energies. The multichance fission probabilities and the corresponding fission times are also obtained, and they are shown to depend sensitively on the shell correction energies and the neutron separation energies of the compound nuclei involved. The experimental neutron multiplicities are reproduced by adjusting the saddle-to-scission transition time interval. An additional delay time for compound nuclear formation is found necessary to fit the experimental neutron multiplicities for a system with higher entrance channel mass symmetry.

DOI: 10.1103/PhysRevC.106.024604

I. INTRODUCTION

The fission of an excited atomic nucleus is a complex process in which the nucleus evolves from spherical or nearly spherical to highly elongated shapes, passes the saddle configuration, and then splits into two fission fragments. The charges and masses of the fission fragments and their kinetic energy distributions are decided during the fission process. An excited nucleus can also evaporate neutrons, light-charged particles, and photons. Fission and evaporation are competing processes in the decay of an excited nucleus, and consequently, a number of nuclei in a given ensemble may not undergo fission but become evaporation residues (ER). Though a large volume of research, both experimental and theoretical, has been carried on different aspects of fission, a comprehensive picture is yet to emerge due to the intricate nature of the process [1]. In the above context, the timescale of fission is of interest in order to understand the dynamical evolution of the different stages of the fission process.

The fission timescale has been deduced from experimental data in the past, mostly from the multiplicities of prescission neutrons emitted by the compound nuclei (CN) formed in heavy-ion-induced fusion-fission reactions [2–4]. Based on the expectation that the number of prescission neutrons can serve as a measure of the fission timescale (neutron clock), the latter are found to be typically of the order of a few tens of zs (1 zs $= 10^{-21}$ s). On the other hand, fission timescales from crystal blocking and K x-ray lifetime measurements (atomic clock) are found to be several orders of magnitude higher than those recorded by the neutron clock [5–9]. It was earlier shown from the statistical model (SM) and the combined dynamical and statistical model calculations of fission lifetime that a number of CN can indeed survive timescales of the order of 1000 zs (or more) before they undergo fission [10–12]. More recently, it was observed from full Langevin dynamical calculations that a considerable time interval can elapse between the emission of the last neutron and fission for a sizable fraction of the compound nuclei [13,14]. This decoupling of the neutron emission and fission timescales suggests that the neutron clock and the atomic clock sample different ranges of the temporal evolution of the fission process.

Theoretical estimates of the fission lifetime were obtained in earlier works with various objectives. The statistical model and the combined dynamical and statistical model calculations were performed to show the presence of long-lifetime fission events in the decay of a compound nucleus [10–12]. The Langevin dynamical calculations were aimed at obtaining the timescale of fission events which give rise to the multiplicity of prescission neutrons, the same as in the experimental data [13,14]. The above calculations considered the fission dynamics to be dissipative in nature, and the dissipation strength was treated as an adjustable parameter. However, dissipation also impacts the fission and ER formation probabilities in addition to the multiplicities of prescission neutrons. It is therefore of interest to find the fission timescales which are consistent with fission or ER cross sections and also prescission neutron multiplicities.

In the transition-state model of nuclear fission, a nucleus is considered to have undergone fission when it evolves to a deformation beyond the transition state or the saddle configuration [15,16]. Evaporation of neutrons, light-charged particles, and γ rays can take place from the compound nucleus as it proceeds towards the saddle point after starting from an equilibrated ground-state configuration. The time required by a CN for its passage from the ground state past the saddle point is termed as the saddle time (τ_{saddle}) in the

---

[*] mkphysics153@gmail.com

[†] Formerly with Physics Group, VECC, Kolkata.

2469-9985/2022/106(2)/024604(13)

present work. In a subsequent time interval ($\tau_{\rm ssc}$), the CN reaches the scission from the saddle configuration [11,17]. The evaporation process continues during this time interval. It is also possible that the onset of fission is delayed by an interval during which period no fission takes place, though particles and gamma rays can be emitted [17]. This delay time can arise if there is a delay in the formation of an equilibrated compound nucleus and is denoted by $\tau_{\rm form}$ here. This formation time arises possibly due to the entrance channel dynamics and accounts for a slower equilibration time of the projectile plus target composite system on its way towards formation of the CN, although thermal equilibration happens on a faster timescale and hence allows evaporation during this time interval [18]. The total fission time ($\tau_{\rm fiss}$) will thus be given as

$$\tau_{\rm fiss} = \tau_{\rm form} + \tau_{\rm saddle} + \tau_{\rm ssc}.$$

Statistical model calculations for heavy-ion-induced fusion-fission reactions which reproduce fission or ER excitation functions are usually found to underestimate the multiplicities of prescission neutrons [19–21]. The time intervals $\tau_{\rm form}$ and $\tau_{\rm ssc}$ have been used in earlier works in order to allow for evaporation of an additional number of neutrons to fit the experimental prescission multiplicities [2,17]. Our objective in the present work is to obtain $\tau_{\rm saddle}$ from statistical model calculations which reproduce the experimental fission or ER excitation functions and $\tau_{\rm form}$ and $\tau_{\rm ssc}$ from fitting the prescission neutron data. The above three time intervals together will give the total fission time, which will be consistent with both fission or ER cross sections and prescission neutron multiplicities.

We perform statistical model calculations for the systems ^{12}C + ^{194,198}Pt, ^{16,18}O + ^{194}Pt, ^{12}C + ^{204}Pb, and ^{19}F + ^{197}Au forming the compound nuclei ^{206,210}Po, ^{210,212}Rn, and ^{216}Ra, respectively, at incident beam energies above the Coulomb barrier. The fission or ER cross sections are calculated in order to fit the experimental excitation functions by adjusting the SM parameters. The corresponding saddle time $\tau_{\rm saddle}$ will also be obtained. Subsequently, the calculated prescission multiplicities are fitted to the experimental values by adjusting the saddle-to-scission time $\tau_{\rm ssc}$ and the delay time $\tau_{\rm form}$. The contribution of different multichance fission to $\tau_{\rm saddle}$ is also obtained. We interpret the results in terms of the neutron separation energy and the various decay widths of the CN.

The details of the statistical model used in the present work are given in the next section. Section III contains the results. A discussion and summary of this work are presented in the last section.

II. STATISTICAL MODEL

The statistical model calculation begins by assuming that a fully equilibrated compound nucleus is formed by the complete fusion of a projectile with the target nucleus. The subsequent decay of the CN by evaporation of light particles, γ rays or fission is decided by the respective decay widths Γ_i ($i = n, p, \alpha, \gamma$) or Γ_f for fission. The time evolution of the CN is followed in small time steps, and the decision whether the CN has undergone any decay process by way of evaporation or fission at each time step is taken by a Monte Carlo sampling using the total decay width $\Gamma_{\rm tot} = \Gamma_n + \Gamma_p + \Gamma_\alpha + \Gamma_\gamma + \Gamma_f$. When a decay is recorded, the type of the decay, i.e., either one of the evaporation channels or fission, is decided by another Monte Carlo sampling of the partial decay widths. The energy and angular momentum carried away by the evaporated particle γ are also obtained by a Monte Carlo method, and the excitation energy and spin of the daughter CN are suitably changed. The time evolution continues until the CN fissions or becomes an evaporation residue (ER). When fission happens, the CN is considered to have just crossed the saddle configuration. The CN is then followed for another time interval $\tau_{\rm ssc}$, in order to allow the CN to evolve from the saddle to the scission configuration. The saddle-to-scission sector is also followed in small time intervals, and the number of evaporated particles and γ is obtained by sampling of evaporation widths as outlined above. The prescission multiplicities of various particles and γ are given by the sum of the emissions in the presaddle and postsaddle sectors. The details of this procedure may be found in [22].

The various decay widths of a CN depend upon its excitation energy (E^*) and spin (ℓ). We obtain the spin distribution of the CN formed in a fusion reaction from coupled-channel calculations using the code CCFULL, where the low-lying collective states of the projectile and target are coupled with the entrance channel relative motion [23]. For a given fusion-fission reaction at a given beam energy, a large ensemble comprised of 200 000 or higher number of compound nuclei is considered. The spin of each CN is assigned by a Monte Carlo sampling of the CCFULL-generated spin distribution, and its time evolution is followed. The final observables, namely, the fission or ER probabilities, prescission multiplicities, and the saddle time, are obtained as averages over all the events in the ensemble.

The particle and γ-decay widths used in the present work are obtained from the Weisskopf formula as given in Ref. [24]. The fission width is taken from the work of Kramers [15] and is given as

$$\Gamma_f(E^*, \ell) = \Gamma_f^{BW}(E^*, \ell)\left(\sqrt{1 + \left(\frac{\beta}{2\omega_s}\right)^2} - \frac{\beta}{2\omega_s}\right), \quad (1)$$

where a dissipative stochastic dynamical model of fission is considered and which consequently gives rise to a reduction from the fission width $\Gamma_f^{BW}(E^*,\ell)$, given by the transition-state theory of Bohr and Wheeler [16]. β is the reduced dissipation coefficient, and ω_s is the frequency of a harmonic oscillator potential, which approximates the potential at the saddle configuration and depends on the spin of the CN [25]. Denoting the component of the CN spin along the symmetry axis by K, the Bohr-Wheeler fission width for $K = 0$ is given as [16]

$$\Gamma_f^{BW}(E^*, \ell, K = 0) = \frac{1}{2\pi\rho_g(E^*, \ell)} \int_0^{E^*-B_f(\ell)} \rho_s[E^* - B_f(\ell) - \epsilon, \ell] d\epsilon, \quad (2)$$

where ρ_g and ρ_s denote the level densities at the ground-state and saddle configurations, respectively, and $B_f(\ell)$ is the angular-momentum-dependent fission barrier. Here, it is assumed that the spin of the CN remains perpendicular to the symmetry axis throughout the course of the reaction. However, the CN spin can be tilted away from the initial direction due to intrinsic nuclear motion resulting in nonzero values of K, which consequently reduces the fission barrier [26]. Assuming a fast equilibration of the K degree of freedom, its effect on fission width can be obtained as [27]

$$\Gamma_f^{BW}(E^*,\ell) = \Gamma_f^{BW}(E^*,\ell,K=0)\frac{K_0\sqrt{2\pi}}{2\ell+1} \times \mathrm{erf}\left(\frac{l+1/2}{K_0\sqrt{2}}\right), \tag{3}$$

with $K_0^2 = \frac{I_{\rm eff}}{\hbar^2}T_{\rm sad}$, and $T_{\rm sad}$ and $I_{\rm eff}$ are the temperature and the effective moment of inertia at the saddle configuration; erf(x) denotes the error function.

The nuclear shell effects in the level density parameter and fission barrier are also taken into account in the present calculations. We use the following level density parameter a, which includes an excitation-energy-dependent shell effect term and is given as [28]

$$a(E_{th}) = \tilde{a}\left(1 + \frac{1-\exp(-E_{th}/E_D)}{E_{th}}\delta\right), \tag{4}$$

where E_{th} is the thermal part of the excitation energy, δ is the shell correction energy, and E_D is a parameter which accounts for the rate of decrease of shell effect with increasing excitation energy. The asymptotic shape-dependent level density parameter $\tilde{a}$ is taken from the work of Reisdorf [29].

The fission barrier after inclusion of shell correction energy can be written as

$$B_f(l) = B_f^{LDM}(l) - (\delta_g - \delta_s), \tag{5}$$

where $B_f^{LDM}(\ell)$ is the angular-momentum-dependent liquid drop model fission barrier [30], and δ_g and δ_s, respectively, denote the shell correction energies for the ground-state and saddle configurations. The deformation-dependent shell correction energies δ_g and δ_s are obtained following the recipe given in Ref. [31], which yields a negligible correction at large deformations, while the full shell correction is applied at zero deformation.

The enhancement of level density at low excitation energies due to collective states is also considered in this work. After inclusion of the collective enhancement of level density (CELD), the total level density $\rho(E^*)$ can be written as [32]

$$\rho(E^*,\ell) = K_{\rm Coll}(E^*,\ell)\rho_{\rm intr}(E^*,\ell), \tag{6}$$

where $K_{\rm Coll}$ is the collective enhancement factor, and $\rho_{\rm intr}$ is the intrinsic level density after inclusion of shell effect. $K_{\rm Coll}$ can have both vibrational and rotational components [33], and a smooth transition from vibrational to rotational enhancement with increasing deformation is obtained from Ref. [34]. A factor accounting for damping of CELD with increasing excitation energy is also included [35]. The total level density thus obtained is used to calculate all the decay widths including fission.

The fission width given by Eq. (1) represents its stationary value, which is reached after a certain time interval in the stochastic dynamical model of fission [36]. We use the following parametrized form of the time-dependent fission width [37],

$$\Gamma_f(E^*,\ell,t) = \Gamma_f(E^*,\ell)\left[1 - \exp^{\frac{-2.3t}{\tau_f}}\right], \tag{7}$$

where

$$\tau_f = \frac{\beta}{2\omega_g^2}\ln\left(\frac{10B_f(\ell)}{T}\right) \tag{8}$$

is the transient time period, and ω_g is the frequency of the harmonic oscillator potential approximating the potential at the ground state. The time interval $\tau_{\rm form}$ mentioned in the previous section is also included and treated as a free parameter in the present calculation. The time t in Eq. (7) is counted after $\tau_{\rm form}$ has elapsed.

The saddle-to-scission transition time interval $\tau_{\rm ssc}$ is obtained from either of the following two considerations. Firstly, it can be used as a free parameter to fit the experimental data. Alternatively, it can be obtained in a dynamical model where the CN moves under a dissipative and repulsive force from the saddle to the scission configuration and is given as [38]

$$\tau_{\rm ssc} = \tau_{\rm ssc}^{o}\left(\sqrt{1+(\frac{\beta_{ss}}{2\omega_s})^2} + \frac{\beta_{ss}}{2\omega_s}\right), \tag{9}$$

where β_{ss} is the dissipation strength in the saddle-to-scission region, and $\tau_{\rm ssc}^{o}$ is the transit time without dissipation [36,38]. The details of the above features can be found in Ref. [20] and are implemented in the statistical model code VECSTAT [39]. Excitation functions of fission or ER and neutron prescission multiplicities are calculated along with the saddle time $\tau_{\rm saddle}$ for a number of reactions and are presented in the next section.

III. CALCULATIONS AND RESULTS

A. Fission or evaporation residue cross sections

We first show the calculated fission cross sections for the fusion-fission reactions ^{12}C + ^{194}Pt and ^{12}C + ^{198}Pt populating the CN ^{206}Po and ^{210}Po, respectively, in Fig. 1. The experimental fission cross sections from Ref. [40] are also shown. The spin distributions of the CN used in the statistical model calculations are obtained by fitting the experimental fusion cross sections [40] using the coupled-channel code CCFULL [23]. It is observed in Fig. 1 that SM results obtained with the dissipation coefficient $\beta = 0$ substantially overestimate the fission cross sections. However, the fission excitation functions for both the reactions can be well reproduced using $\beta = 1.5\,{\rm zs}^{-1}$ and $3\,{\rm zs}^{-1}$ for the ^{12}C + ^{194}Pt and ^{12}C + ^{198}Pt reactions, respectively. The statistical model results for evaporation residue (ER) excitation functions for the reactions ^{16}O + ^{194}Pt and ^{18}O + ^{194}Pt, forming the compound nuclei ^{210}Rn and ^{212}Rn, respectively, are given in Fig. 2 and compared with the experimental cross sections [41,42]. The fusion cross sections to generate CN spin distributions are taken from Refs. [42,43]. The SM considerably underpredicts the ER cross sections with $\beta = 0$. Reasonably good fits are obtained for the reactions ^{16}O + ^{194}Pt and ^{18}O + ^{194}Pt with $\beta = 1.5\ {\rm zs}^{-1}$ and $2.5\ {\rm zs}^{-1}$, respectively.

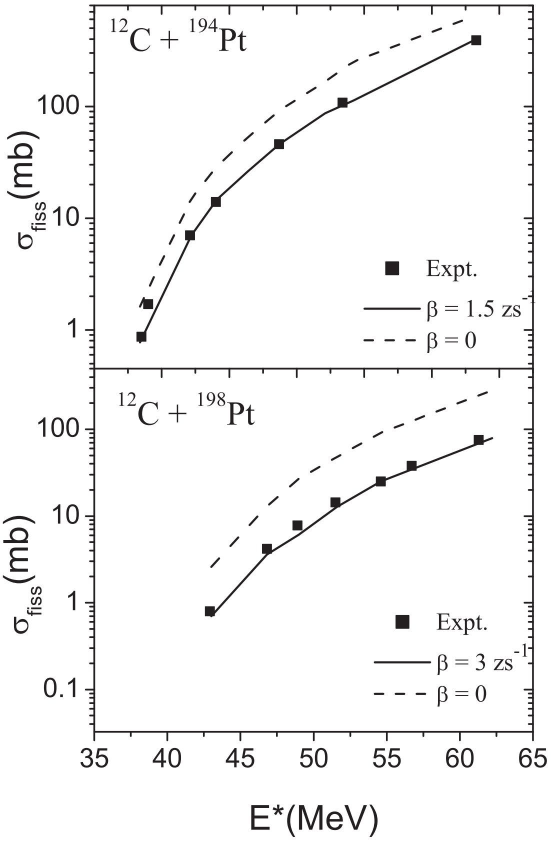

FIG. 1. The fission cross sections (σ_{fiss}) for the reactions $^{12}\text{C} + ^{194}\text{Pt}$ and $^{12}\text{C} + ^{198}\text{Pt}$ forming the compound nuclei ^{206}Po and ^{210}Po, respectively. Statistical model results with $\beta = 0$ and best-fit values are shown. The experimental points are from Ref. [40].

Lastly, we consider the reactions $^{12}\text{C} + ^{204}\text{Pb}$ and $^{19}\text{F} + ^{197}\text{Au}$ which form the same compound nucleus ^{216}Ra. These reactions were studied extensively by Berriman *et al.* [44], who observed fusion suppression for the $^{19}\text{F} + ^{197}\text{Au}$ reaction by comparing the reduced ER cross sections for the two systems. Following Ref. [44], we also consider evaporation residues comprised of only Ra isotopes in order to avoid residues formed by incomplete fusion of the projectile with the target. The reduced ER excitation function for the $^{12}\text{C} + ^{204}\text{Pb}$ can be fitted by using $\beta = 2.2\ \text{zs}^{-1}$ in the present calculation (Fig. 3). Since both the reactions under discussion lead to the same CN, the excitation function for $^{19}\text{F} + ^{197}\text{Au}$ is also calculated using the above value of β. This excitation function, however, overestimates the experimental data and merges with the calculated excitation function for $^{12}\text{C} + ^{204}\text{Pb}$ at higher excitation energies, similar to the observation made in Ref. [44].

We may add here that the same dissipation strengths are used for the ^{216}Ra compound nuclei populated in the two reactions, though their spin distributions are different. In fact, spin distributions deduced from the experimental fusion cross sections show that slightly lower spin states are populated in the $^{19}\text{F} + ^{197}\text{Au}$ reaction than the $^{12}\text{C} + ^{204}\text{Pb}$ reaction, in spite of ^{19}F being the heavier projectile due to the difference in barrier distributions in the two reactions [44]. In principle,

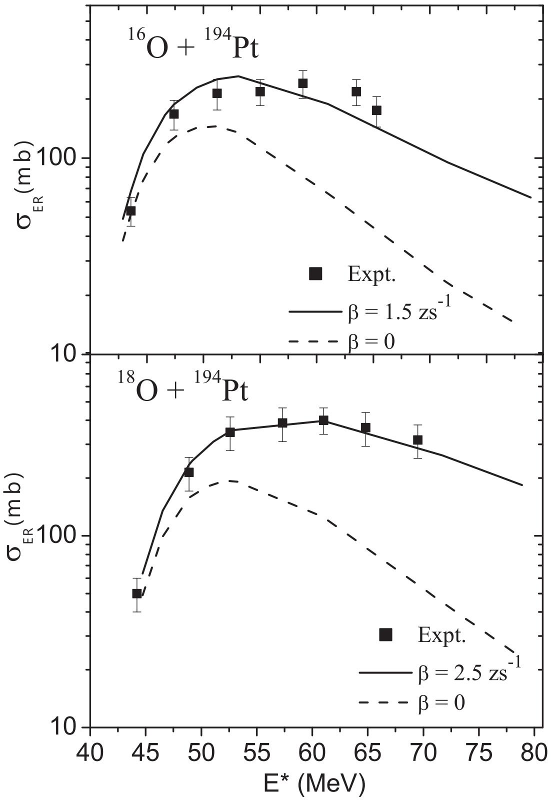

FIG. 2. The evaporation residue cross sections (σ_{ER}) for the reactions $^{16}\text{O} + ^{194}\text{Pt}$ and $^{18}\text{O} + ^{194}\text{Pt}$ forming the compound nuclei ^{210}Rn and ^{212}Rn, respectively. Statistical model results with $\beta = 0$ and best-fit values are shown. The experimental points are from Refs. [41,42].

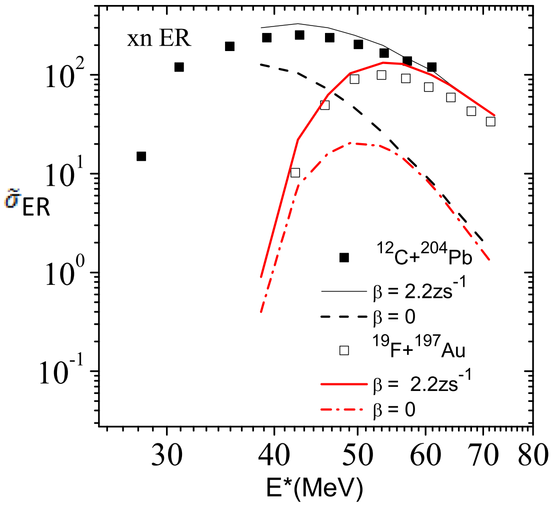

FIG. 3. The reduced evaporation residue cross sections $\tilde{\sigma}_{ER} = \sigma_{ER}/\pi\ \lambda\!\!\!^{-}{}^2$ where $\lambda\!\!\!^{-}$ is the de Broglie wavelength in the entrance channel, for the reactions $^{12}\text{C} + ^{204}\text{Pb}$ and $^{19}\text{F} + ^{197}\text{Au}$, both forming the compound nucleus ^{216}Ra. Statistical model results with $\beta = 0$ and $2.2\ \text{zs}^{-1}$ are shown. The experimental points are from Ref. [44].

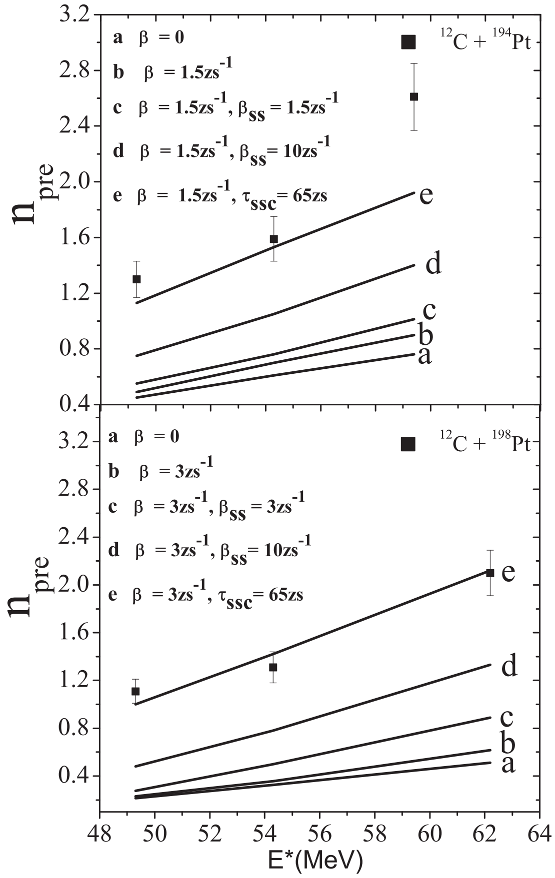

FIG. 4. The prescission neutron multiplicities (n_{pre}) for the reactions $^{12}\text{C} + {}^{194}\text{Pt}$ and $^{12}\text{C} + {}^{198}\text{Pt}$, forming the compound nuclei ^{206}Po and ^{210}Po, respectively. Statistical model results for presaddle neutrons obtained with $\beta = 0$ and best-fit β values from fission excitation functions are shown (lines a and b, respectively). Lines c and d show n_{pre} values which include saddle-to-scission contributions obtained with $\beta = \beta$ (best-fit) and $\beta_{ss} = 10\ \text{zs}^{-1}$, respectively. n_{pre} values calculated with β (best-fit) and $\tau_{\text{ssc}} = 65\,\text{zs}$ are given by the line e. The experimental points are from Ref. [46].

the one-body dissipation can depend upon nuclear spin, but little is known about this dependence [45]. So we use the same values for both the dissipation coefficients β and β_{ss} in both reactions in the SM calculations.

B. Prescission neutron multiplicities

We next present the statistical model results for prescission neutron multiplicity (n_{pre}) obtained for the reactions under consideration. Figure 4 shows the calculated n_{pre} values for the $^{12}\text{C} + {}^{194}\text{Pt}$ and $^{12}\text{C} + {}^{198}\text{Pt}$ reactions forming the compound nuclei ^{206}Po and ^{210}Po, respectively, for various input parameters. The numbers of presaddle neutrons obtained with $\beta = 0$ and $1.5\,\text{zs}^{-1}$ are considerably smaller than the experimental results [46]. When neutrons emitted during the saddle-to-scission transition are taken into account [Eq. (9)], n_{pre} remains underpredicted when $\beta = \beta_{ss} = 1.5\,\text{zs}^{-1}$ are used in the statistical model calculations, though $\beta = 1.5\,\text{zs}^{-1}$ gives good fit to the fission excitation function (Fig. 1). Statistical model results with $\beta = 1.5\,\text{zs}^{-1}$ and $\beta_{ss} = 10\,\text{zs}^{-1}$ are still lower than the experimental multiplicities. Similarly, observations are made for the $^{12}\text{C} + {}^{198}\text{Pt}$ reaction, where $\beta = 3\ \text{zs}^{-1}$ is used, since it well reproduces the experimental fission cross sections. n_{pre} obtained with $\beta = 3\ \text{zs}^{-1}$ and $\beta_{ss} = 10\ \text{zs}^{-1}$ in this case also fall short of the experimental values.

In the context of the choice of values for β or β_{ss}, we would like to point out that the dissipation strength represents the coupling between the intrinsic and collective nuclear degrees of freedom, giving rise to an irreversible energy flow from the collective to the intrinsic motion. Theoretical estimates of one-body nuclear dissipation, which is mostly used in low-energy nuclear dynamics, are not quite specific as yet. While macroscopic models predict an excitation energy independent one-body dissipation [47], microscopic calculations show a strong dependence on excitation energy which approaches the macroscopic values in the limit of large excitations [48]. One-body dissipation strength also depends on the nuclear shape [47,48], and in particular, a suppression of one-body dissipation strength is predicted when chaos in the single-particle motion is taken into account [49]. All the above considerations led us to treat both β or β_{ss} as adjustable parameters where they can assume different values since they represent dissipation for different domains of nuclear deformation, namely, the presaddle and saddle-to-scission stages. Further, we restrict the choice of the dissipation strengths within the macroscopic predictions of one-body dissipation, since the macroscopic estimates represent the upper limit of one-body dissipation. Hence we do not use β_{ss} values greater than $10\ \text{zs}^{-1}$ which is the macroscopic one-body dissipation strength at large deformations [47]. Alternatively, we use the saddle-to-scission transition time interval τ_{ssc} as an adjustable parameter and calculate the number of neutrons emitted during this period. We find in Fig. 4 that experimental n_{pre} values for both reactions can be reasonably well reproduced (except at the highest energy for the CN ^{206}Po) with $\tau_{\text{ssc}} = 65\,\text{zs}$. Results of similar calculations of n_{pre} for the reactions $^{16}\text{O} + {}^{194}\text{Pt}$ and $^{18}\text{O} + {}^{194}\text{Pt}$ leading to the compound nuclei ^{210}Rn and ^{212}Rn, respectively, are given in Fig. 5. Here, also we find that the number of presaddle neutrons obtained with the β values which reproduce the ER excitation functions are much smaller than the experimental n_{pre}. When saddle-to-scission neutrons are included first using $\beta_{ss} = \beta$ and then $\beta_{ss} = 10\,\text{zs}^{-1}$, n_{pre} still remains underestimated. Reasonable fits to experimental n_{pre} for both the systems are obtained with $\tau_{\text{ssc}} = 65\,\text{zs}$.

We next studied the prescission neutron multiplicities emitted by the compound nucleus ^{216}Ra populated through two different entrance channels $^{12}\text{C} + {}^{204}\text{Pb}$ and $^{19}\text{F} + {}^{197}\text{Au}$. Observations similar to those made for the systems as given above are also made here, as shown in Fig. 6. Interestingly, though experimental n_{pre} values are well reproduced with $\tau_{\text{ssc}} = 65\,\text{zs}$ for $^{12}\text{C} + {}^{204}\text{Pb}$, it is underestimated to some extent for $^{19}\text{F} + {}^{197}\text{Au}$ with the same value of τ_{ssc}. The underestimation of n_{pre} for $^{19}\text{F} + {}^{197}\text{Au}$ with respect to $^{12}\text{C} + {}^{204}\text{Pb}$ is possibly due to the higher symmetry of the entrance channel of the former system compared to the latter. A suppression of the reduced ER cross sections for the $^{19}\text{F} + {}^{197}\text{Au}$ system with respect to the statistical model predictions has been observed

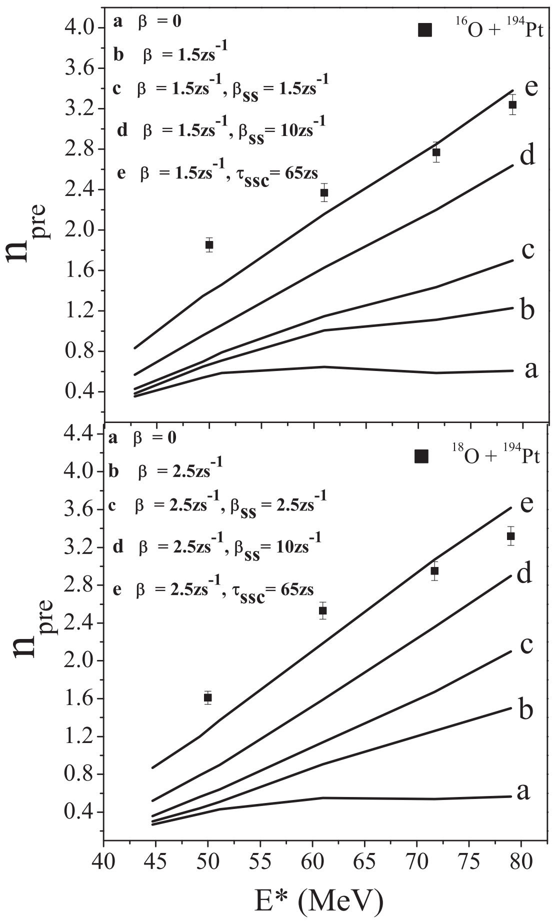

FIG. 5. The prescission neutron multiplicities (n_{pre}) for the reactions $^{16}\mathrm{O}+{}^{194}\mathrm{Pt}$ and $^{18}\mathrm{O}+{}^{194}\mathrm{Pt}$, forming the compound nuclei ^{210}Rn and ^{212}Rn, respectively. Statistical model results for presaddle neutrons obtained with $\beta = 0$ and best-fit β values from ER excitation functions are shown (lines a and b, respectively). Lines c and d shows n_{pre} values which include saddle-to-scission contributions obtained with $\beta(best\text{-}fit)$ and $\beta_{ss} = 10\,\mathrm{zs}^{-1}$, respectively. n_{pre} values calculated with $\beta(best\text{-}fit)$ and $\tau_{\mathrm{ssc}} = 65$ zs are given by the line e. The experimental points are from Ref. [51].

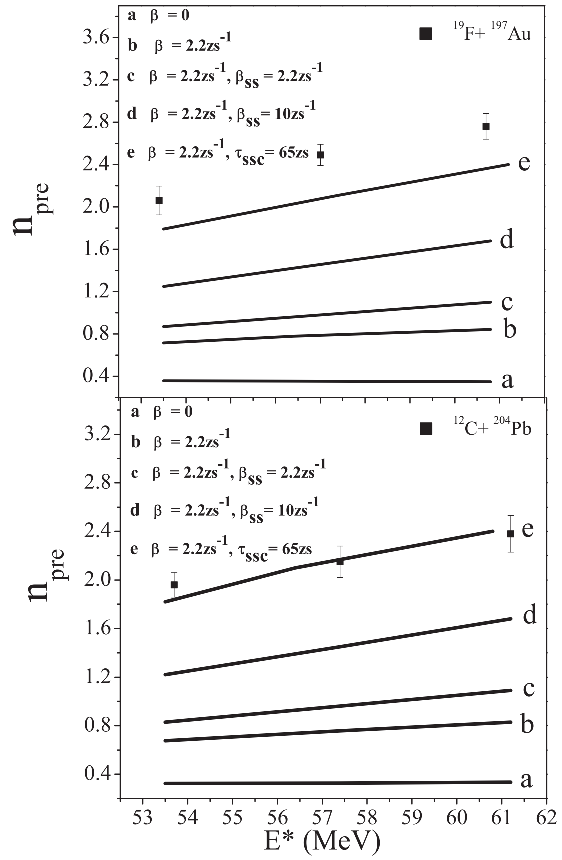

FIG. 6. The prescission neutron multiplicities (n_{pre}) for the reactions $^{12}\mathrm{C}+{}^{204}\mathrm{Pb}$ and $^{19}F+{}^{197}\mathrm{Au}$, both forming the compound nucleus ^{216}Ra. Statistical model results for presaddle neutrons obtained with $\beta = 0$ and best-fit β values from ER excitation functions are shown (lines a and b, respectively). Lines c and d show n_{pre} values, which include saddle-to-scission contributions obtained with $\beta(best\text{-}fit)$ and $\beta_{ss} = 10\,\mathrm{zs}^{-1}$, respectively. n_{pre} values calculated with $\beta(best\text{-}fit)$ and $\tau_{\mathrm{ssc}} = 65$ zs are given by line e. The experimental points are from Ref. [52].

earlier [44] and also in the present work (Fig. 3) and has been attributed to the diversion of a part of the entrance channel flux to quasifission, though none has been observed for the $^{12}\mathrm{C}+{}^{204}\mathrm{Pb}$ system. Therefore the entrance channel dynamics is expected to be quite different for the two systems. While the projectile nucleus can be swallowed by the target nucleus to form the compound nucleus in the less symmetric $^{12}\mathrm{C}+{}^{204}\mathrm{Pb}$ system, a considerable amount of mass flow from the target to the projectile nucleus will take place before they fuse to form the compound nucleus for the more symmetric $^{19}\mathrm{F}+{}^{197}\mathrm{Au}$ system. No fission takes place during this formation time interval τ_{form}, already introduced in Sec. I, though the particles and γ can be evaporated. It is to be noted here that the CN is not necessarily in a spherical equilibrated configuration at the end of the interval τ_{form} but can assume a symmetrical dinuclear shape [50]. The transient time period given in Eq. (8) considers all CN to start with a spherical shape and evolve to the saddle configuration and hence cannot give an accurate time dependence of the fission width when the initial shape is nonspherical. In such cases, Langevin dynamical calculations have shown that the time dependence of the fission width alters from Eq. (7) in the transient region with a shortening of the transient time [50]. In the present case, the transient time from Eq. (8) is of the order of 10 zs or less and can serve as an upper limit of the error in the estimation of transient time due to noninclusion of nonspherical initial shapes. This interval being small in comparison with other timescales, we continue using Eqs. (7) and (8) in SM calculations.

Statistical model calculations are performed for the $^{19}\mathrm{F}+{}^{197}\mathrm{Au}$ system, where τ_{form} is included as an adjustable parameter. The results for n_{pre} are shown in Fig. 7, where we find that experimental multiplicities can be well reproduced with $\tau_{\mathrm{form}} = 30\,\mathrm{zs}$. It may be noted, however, that though the presaddle contribution to n_{pre} increases with introduction of τ_{form} as expected, it also reduces the available excitation energy in the saddle-to-scission sector. Consequently, the saddle-to-scission contribution decreases though the total multiplicity increases. Formation time intervals of similar

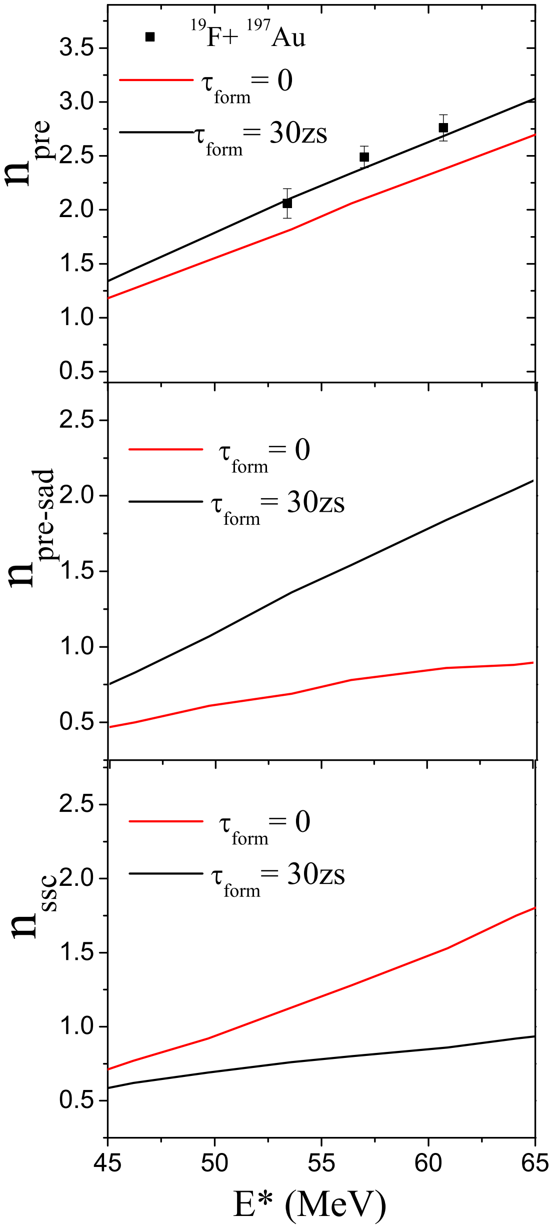

FIG. 7. Prescission neutron multiplicity ($n_{\rm pre}$) obtained with $\tau_{\rm form}$. The presaddle ($n_{\rm pre-sad}$) and saddle-to-scission ($n_{\rm ssc}$) contributions to $n_{\rm pre}$ are also shown.

orders of magnitude have also been found in earlier works [18,53,54]. Introducing a formation time, however, also affects the ER cross sections. The reduced ER cross sections for $^{19}\mathrm{F}+{}^{197}\mathrm{Au}$ obtained with $\tau_{\rm form}=30$ zs are given in Fig. 8. Evaporation during $\tau_{\rm form}$ depletes the excitation energy, which consequently increases the ER cross sections, as observed in Fig. 8. Further, it is also likely that the number of neutrons emitted in quasifission events is smaller than those from CN fission, since the timescale of the former is expected to be shorter than the latter. Therefore, on the one hand, a long formation time for the CN increases the neutron multiplicity, while the quasifission events reduce the neutron multiplicity on the other. We observe here a net increase of neutron multiplicity from the $^{19}\mathrm{F}+{}^{197}\mathrm{Au}$ reaction compared to a less symmetric system. Evidently, detailed calculations of entrance channel dynamics would be required in order to make further quantitative assessment of neutron emission during the formation stage and from quasifission events.

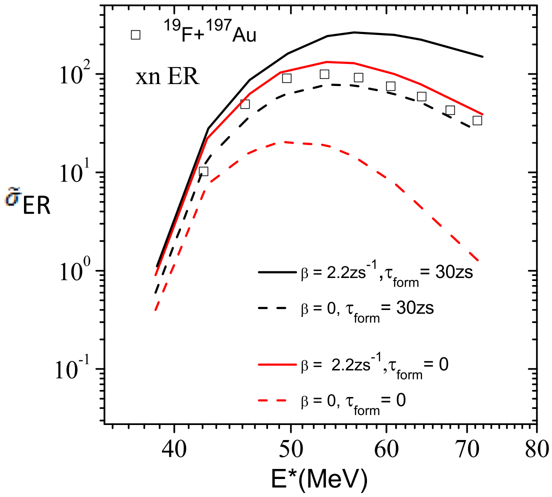

FIG. 8. Effect of formation time delay ($\tau_{\rm form}$) on reduced ER cross section.

A number of observations can be made regarding the dependences of fission or ER cross sections and $n_{\rm pre}$ on the dissipation strength β. The fission or ER cross sections change substantially when β is increased from 0 to (1.5–3.0) zs^{-1} for the compound nuclei ^{206,210}Po, ^{210,212}Rn, and ^{216}Ra (Figs. 1–3). The corresponding increase of $n_{\rm pre}$ with increase of β is however marginal for ^{206,210}Po over the entire range of excitation energy considered here. The β dependence of $n_{\rm pre}$ increases with excitation energy for ^{210,212}Rn and is strong over the entire excitation energy range for ^{216}Ra. The above observations can be qualitatively understood as follows.

The fission and presaddle neutron emission probabilities of a CN are given as $P_f=\Gamma_f/(\Gamma_f+\Gamma_n)$ and $P_n=\Gamma_n/(\Gamma_f+\Gamma_n)$, where Γ_f and Γ_n are the fission and neutron widths, respectively. The charged particle and photon emission widths are much smaller than Γ_n and hence are not included here for the sake of simplification, though they are included in the SM calculations. Denoting Γ_f/Γ_n by x, P_f and P_n can be written as $P_f=x/(x+1)$ and $P_n=1/(x+1)$. When the dissipation strength β increases, Γ_f and hence x decrease [Eq. (1)]. If $x<1$, P_f changes substantially with x, while the effect on P_n is marginal. This is the case with ^{206,210}Po, for which $x<1$ over the energy range under study, as shown in Fig. 9. On the other hand, P_f depends weakly on x when $x>1$, but the dependence of P_n is strong. However, large x implies a large fission cross section and consequently low ER cross section. Therefore a small change in fission cross section will make a large fractional change in ER cross section. Thus both ER cross section and $n_{\rm pre}$ will be sensitive to β, which is observed at higher excitation energies for ^{210,212}Rn, where $x>1$ and at all excitation energies for ^{216}Ra (Fig. 9).

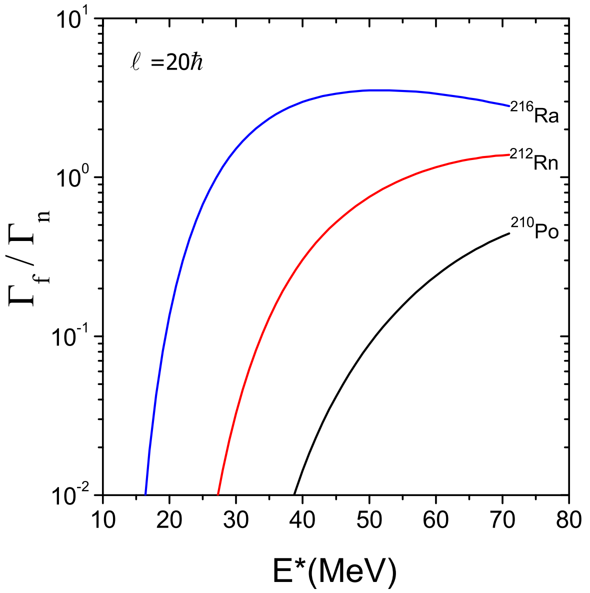

FIG. 9. Fission-to-neutron width ratios for the compound nuclei ^{210}Po, ^{212}Rn, and ^{216}Ra at CN spin ℓ of $20\hbar$. The width ratios for ^{206}Po and ^{210}Rn are higher than ^{210}Po and ^{212}Rn, respectively, and are not shown here.

C. The saddle-time scale

When a fission event is recorded in the SM calculations, the CN is considered to have just crossed the fission barrier. The elapsed time interval termed as the saddle time is introduced in Sec. I. The distribution of the saddle time for a large (500 000) ensemble of compound nuclei for the $^{12}\mathrm{C}+{}^{204}\mathrm{Pb}$ system at $E^* = 56$ MeV is displayed in Fig. 10. It is interesting to note that though the average saddle time is 259 zs, quite a few fission events with time scale of 10 000 zs are recorded, similar to the earlier observation by Morjean *et al.* [10] and more recently by Rai *et al.* [14]. The ensemble average value of the saddle time will be denoted by τ_{saddle} for further discussions. The τ_{saddle} obtained for the various systems are shown in Figs. 11–13.

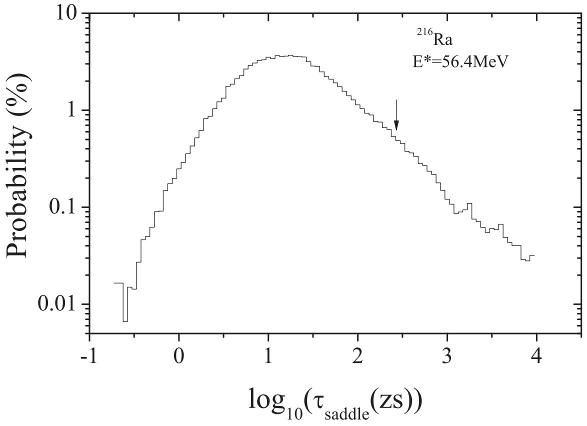

FIG. 10. Saddle-time distribution of the compound nucleus ^{216}Ra populated in the $^{12}\mathrm{C}+{}^{204}\mathrm{Pb}$ reaction. The average saddle time (259 zs) is marked by the arrow.

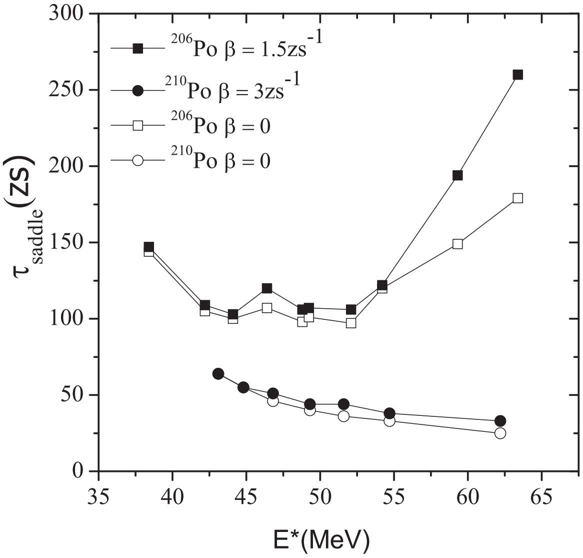

FIG. 11. The excitation energy dependence of the average saddle time (τ_{saddle}) of ^{206}Po and ^{210}Po compound nuclei obtained with $\beta = 0$ and also with the β that best fits the respective fission excitation functions.

It is observed from the above figures that τ_{saddle} increases with β by varying degrees for different systems. While τ_{saddle} increases marginally with β at all E^* for ^{210}Po, the increase is small at low E^* but large at high E^* for ^{206}Po. For both ^{210,212}Rn compound nuclei, the β sensitivity of τ_{saddle} is small low E^* but increases at higher E^*. τ_{saddle} depends strongly on β for ^{216}Ra at all E^*. In order to understand these observations, we proceed as follows.

The average lifetime of a CN is given by $1/\Gamma_t$, where $\Gamma_t = \Gamma_f + \Gamma_n$, and the other evaporation widths (light-charged

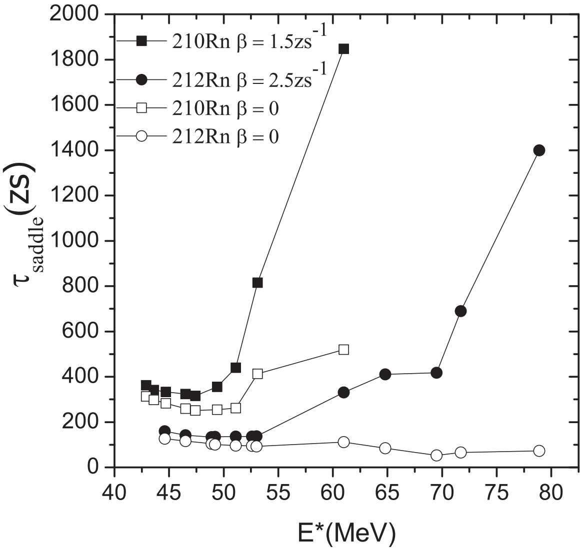

FIG. 12. The excitation energy dependence of the average saddle time (τ_{saddle}) of ^{210}Rn and ^{212}Rn compound nuclei obtained with $\beta = 0$ and also with the β that best fits the respective ER excitation functions.

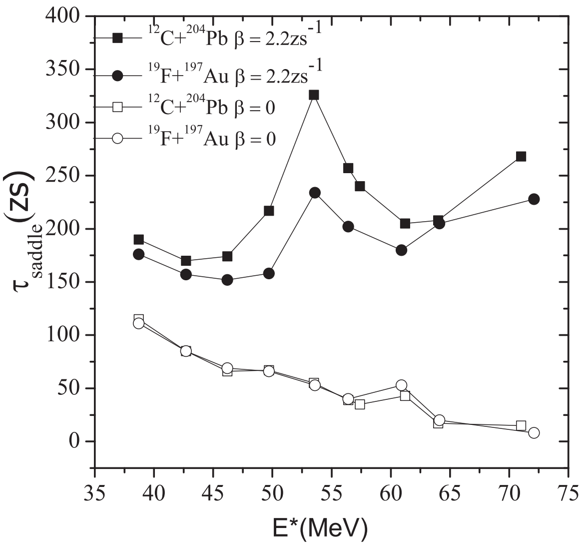

FIG. 13. The excitation energy dependence of the average saddle time ($\tau_{\rm saddle}$) of the compound nucleus ^{216}Ra populated through the $^{12}\mathrm{C} + {}^{204}\mathrm{Pb}$ and $^{19}\mathrm{F} + {}^{197}\mathrm{Au}$ reactions obtained with $\beta = 0$ and 2.2 zs^{-1}.

particles and γ) are not considered for simplification. If the CN undergoes first chance fission, then the saddle-time scale is also given by $1/\Gamma_t$. In the event of a neutron emission, the daughter CN can still undergo second or higher chance fission after emission of more neutrons. The saddle time is then given as the weighted average of the lifetime of the compound nuclei populated after each neutron emission. Since the fission width Γ_f decreases with increasing dissipation strength β, the CN lifetime $[1/(\Gamma_f + \Gamma_n)]$ also increases with increasing β. However, if $\Gamma_f \ll \Gamma_n$ or $\Gamma_f/\Gamma_n \ll 1$, the increase in CN lifetime is marginal with increase in β. This is the case for ^{210}Po, where $\Gamma_f/\Gamma_n \ll 1$ as shown in Fig. 14, and consequently, $\tau_{\rm saddle}$ increases only marginally with β (Fig. 11). As Γ_f/Γ_n increases, the β dependence of $\tau_{\rm saddle}$ also increases. This happens for ^{206}Po, where Γ_f/Γ_n increases from small values ($\ll 1$) at low E^* to larger values ($\backsim 1$) at higher excitation energies. Consequently, β dependence of $\tau_{\rm saddle}$ is weak at low excitation energies and becomes stronger at high excitation energies. The cases for ^{210,212}Rn are similar, where Γ_f/Γ_n increases from smaller to larger values with increasing E^* (Fig. 9), which causes increasing β sensitivity of $\tau_{\rm saddle}$ with increasing E^* (Fig. 12). For ^{216}Ra, $\Gamma_f/\Gamma_n > 1$ for the energy interval under study (Fig. 9), and this is reflected in a strong β dependence of $\tau_{\rm saddle}$ over the entire excitation energy range (Fig. 13).

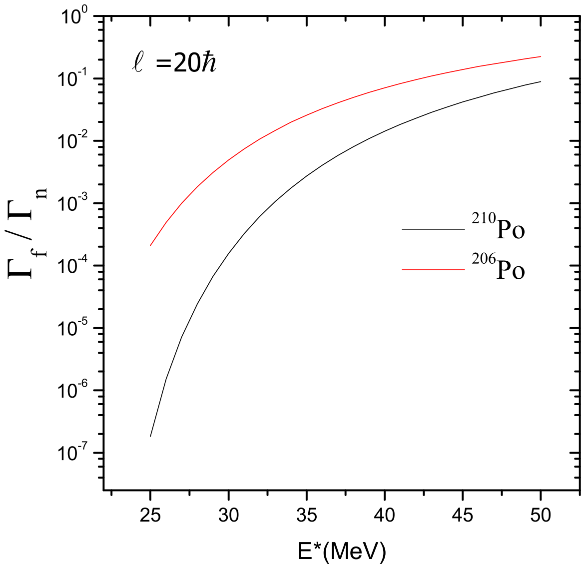

FIG. 14. Fission-to-neutron width ratios for the compound nuclei ^{206}Po and ^{210}Po for CN spin ℓ of $20\hbar$.

Our next observation concerns the excitation energy dependence of $\tau_{\rm saddle}$. It is found in Figs. 11–13 that $\tau_{\rm saddle}$ obtained with $\beta > 0$ has a decreasing trend at lower excitation energies and then it starts increasing with increasing E^* for ^{206}Po, ^{210,212}Rn, and ^{216}Ra compound nuclei. $\tau_{\rm saddle}$ obtained with $\beta = 0$ shows a decreasing trend over the entire energy range for ^{212}Rn and ^{216}Ra, while it shows a decreasing followed by an increasing trend for ^{206}Po and ^{210}Rn compound nuclei. However, $\tau_{\rm saddle}$ for ^{210}Po shows only a decreasing trend with increasing E^* for both values of β. In order to qualitatively explain the above observations, the chance distribution of fission events and the corresponding saddle-time intervals are obtained for the ^{206,210}Po compound nuclei and will be discussed here in some detail. The excitation functions of the ith chance relative fission probability of ^{206,210}Po are displayed in Fig. 15. Here, the first chance relative fission probability corresponds to the fraction of the events where fission takes place before any neutron (or any other particle) emission, and similarly, the second chance fission refers to fission after emission of one neutron and so forth. It is observed that the first chance relative fission probability for ^{210}Po is higher than ^{206}Po, and consequently second and higher chance relative fission probabilities for ^{210}Po are smaller than those of ^{206}Po. The chance dependence of relative fission probabilities at various excitation energies is given in Fig. 16. The higher chance fission events are found to be rarer than those of lower chance events. The lower chance fission probability, however, decreases with excitation energy, while the higher chance fission probability increases. The decrease of chance probability with chance number can be accounted for by the dependence of the fission probability P_f on E^*, where $P_f = x/(x+1)$, which decreases with decreasing x and $x = \Gamma_f/\Gamma_n$. Since each neutron emission reduces the excitation energy of the daughter CN by about 8 MeV and Γ_f/Γ_n decreases with E^* (Fig. 14), the probability of higher chance fission reduces. The higher first chance relative fission probability of ^{210}Po compared to ^{206}Po can be traced back to the different E^* dependence of Γ_f/Γ_n of the two compound nuclei. As shown in Fig. 14, Γ_f/Γ_n decreases faster for ^{210}Po than ^{206}Po with decreasing E^*. Since higher chance fission events occur at lower E^* than first chance fission, the relative probability of higher chance fission compared to first chance fission is smaller for ^{210}Po than ^{206}Po. This results in a higher relative probability of first chance fission of ^{210}Po compared to ^{206}Po. Consequently, higher chance fission events contribute more to the $\tau_{\rm saddle}$ of ^{206}Po compared to ^{210}Po, resulting in larger

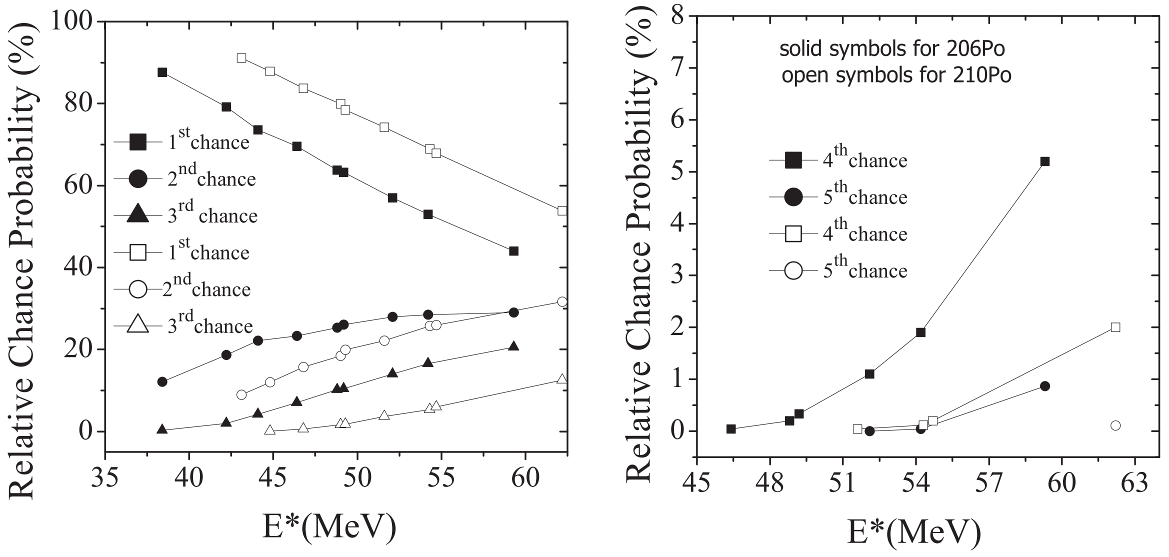

FIG. 15. The excitation energy dependence of the relative probability of various chance fission events for the compound nuclei ^{206}Po and ^{210}Po.

values of τ_{saddle} of the former than the latter, as is observed in Fig. 11.

We next discuss the excitation functions of the saddle time τ^i_{saddle} for different chance (i) fission of ^{206}Po and ^{210}Po compound nuclei as given in Fig. 17. It is found that τ^i_{saddle} decreases with increasing E^* for a given i, which is expected due to the increase of total width Γ_t with E^*. Further, τ^i_{saddle} increases with i for a given initial excitation energy E^*, which reflects the reduced availability of excitation energy for higher chance fission.

It is also observed that the increase of τ^i_{saddle} with i is higher for ^{206}Po than ^{210}Po. The saddle time τ^i_{saddle} of ith chance fission is given by $1/(\Gamma_f + \Gamma_n)$, where Γ_f and Γ_n are the fission and neutron widths of the daughter nucleus populated after evaporation of $(i-1)$ neutrons. While the fission barrier of ^{206}Po is lower than ^{210}Po, the neutron separation energy of the former is higher than that of the latter, as given in Table I. Therefore the effect of higher fission width of ^{206}Po is compensated to some extent by its lower neutron width compared to ^{210}Po. The same is true for ^{205}Po in comparison to ^{209}Po and for other daughter nuclei formed after successive neutron emission. However, the excitation energies of the daughter nuclei from ^{206}Po are smaller than those from ^{210}Po by about 0.6 MeV on average at each stage of evaporation on account of the higher neutron separation energies of the former than the latter. This lowering of excitation energy causes decrease of the widths and hence increase of fission time. All the above factors make τ^i_{saddle} of ^{206}Po larger than ^{210}Po for higher chance fission.

TABLE I. Shell corrected fission barrier and neutron separation energies for isotopes of polonium.

Nucleus	Shell corrected fission barrier (MeV) for $\ell = 0$	Neutron separation energy (MeV)
^{210}Po	21.8	7.66
^{209}Po	21.5	6.97
^{208}Po	20.5	8.40
^{207}Po	19.6	7.03
^{206}Po	18.5	8.74
^{205}Po	17.4	7.25
^{204}Po	16.3	9.10
^{203}Po	15.3	7.44

The total saddle time τ_{saddle} is the average of all τ^i_{saddle} weighted by the respective chance probabilities. At lower excitation energies, first chance fission probability makes the largest contribution to τ_{saddle} and consequently, τ_{saddle} has similar E^* dependence as τ^1_{saddle}. With increasing excitation energy, higher chance fission events start contributing to τ_{saddle}, causing a change in its E^* dependence. If τ^i_{saddle} increases substantially with i, then τ_{saddle} can start increasing with E^*. This happens for ^{206}Po as shown in Fig. 11. On the other hand, both the saddle time and probability of higher chance fission are smaller for ^{210}Po than ^{206}Po (Figs. 17 and 15). As a result, no increase of τ_{saddle} with E^* is noticed for ^{210}Po. Thus, the excitation energy dependence of τ_{saddle} is strongly influenced by the chance distribution and the saddle time of higher chance fission events.

IV. SUMMARY AND DISCUSSIONS

In the present work we have performed statistical model calculations for the systems $^{12}\text{C} + {}^{194,198}\text{Pt}$, $^{16,18}\text{O} + {}^{194}\text{Pt}$, $^{12}\text{C} + {}^{204}\text{Pb}$, and $^{19}\text{F} + {}^{197}\text{Au}$, leading to the compound nuclei ^{206,210}Po, ^{210,212}Rn, and ^{216}Ra. The prescission neutron multiplicities, fission or ER cross sections, and the saddle times of the above reactions are obtained. The dissipation strength β is the only adjustable parameter to reproduce fission or ER excitation functions. While the excitation functions of fission or ER cross sections of the systems under study can be fitted to the experimental data with β values in the range (1.5–3.0)

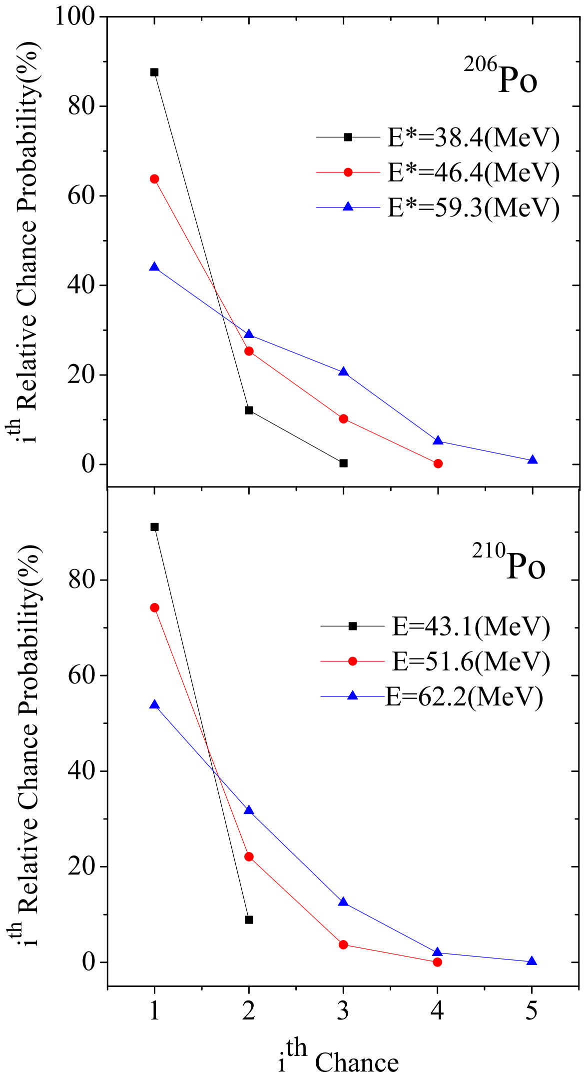

FIG. 16. The chance number dependence of the relative probability of various chance fission events for the compound nuclei ^{206}Po and ^{210}Po.

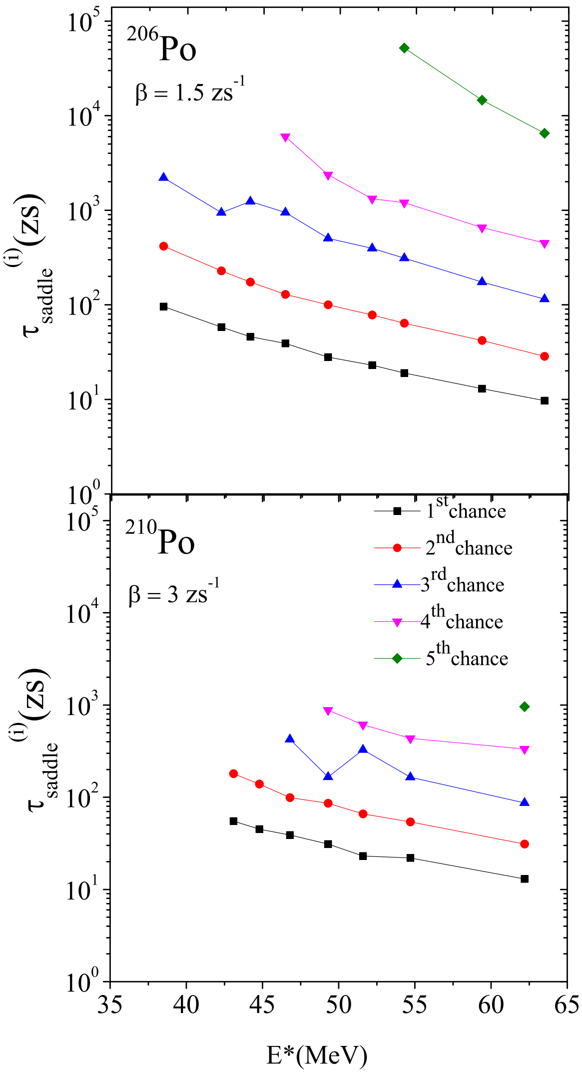

FIG. 17. The excitation energy dependence of saddle time of various chance fission events for the compound nuclei ^{206}Po and ^{210}Po.

zs^{-1}, the prescission neutron multiplicities are underestimated. A saddle-to-scission transition time is used to allow additional neutrons to evaporate to fit the experimental multiplicities. It turns out that a saddle-to-scission transition time of 65 zs is adequate for all the systems except for ^{19}F + ^{197}Au, where quasifission events are known to be present [44]. An additional formation time of 30 zs is required to reproduce the experimental multiplicities of the ^{19}F + ^{197}Au system. Further, investigations are necessary to find the role of dynamics during the formation of the compound nucleus and saddle-to-scission transition in contributing to the total multiplicity of prescission neutrons. The calculated fission or ER cross sections and neutron multiplicities for different systems are found to depend on the dissipation strength differently. This is explained in terms of the different magnitudes and different excitation energy dependence of the Γ_f/Γ_n values of the different systems. It may be mentioned here that Γ_f/Γ_n can also be adjusted by tuning the level density and fission barrier. Simultaneous reproduction of fission or ER cross sections and prescission neutron multiplicities has been reported where two adjustable parameters are used which effectively control the level density and the fission barrier [26,55].

The average saddle times τ_{saddle} for different systems are obtained with β values which best fit the fission or ER excitation functions as well as with $\beta = 0$. The distribution of saddle time among a large number of compound nuclei shows survival of a few nuclei up to 10 000 zs. τ_{saddle} is found to vary from system to system and also depends upon the dissipation strength and the excitation energy of CN. The β dependence of τ_{saddle} is shown to be related to the Γ_f/Γ_n values of the system. The relative probabilities of various chance fission events and their saddle times of the compound nuclei ^{206,210}Po are shown to give rise to the system and excitation energy dependence of τ_{saddle} of the two compound nuclei. The relative probability of a given chance fission event and its saddle time depend sensitively on the fission and neutron widths, which in turn depend upon the shell effects on the level density, fission barrier, and the neutron separation energies. This accounts for the different excitation energy and system dependence of τ_{saddle} as is observed in the present work.

ACKNOWLEDGMENTS

One of us (R.K.) would like to thank the Inter University Accelerator Centre, New Delhi for financial assistance under Grant No. UFR-59306.

---

[1] M. Bender, R. Bernard, G. Bertsch, S. Chiba, J. Dobaczewski, N. Dubray, S. A. Giuliani, K. Hagino, D. Lacroix, Z. Li, P. Magierski, J. Maruhn, W. Nazarewicz, J. Pei, S. Péru, N. Pillet, J. Randrup, D. Regnier, P.-G. Reinhard, L. M. Robledo, W. Ryssens, J. Sadhukhan *et al.*, J. Phys. G: Nucl. Part. Phys. **47**, 113002 (2020)

[2] D. J. Hinde, H. Ogata, M. Tanaka, T. Shimoda, N. Takahashi, A. Shinohara, S. Wakamatsu, K. Katori, and H. Okamura, Phys. Rev. C **39**, 2268 (1989).

[3] D. J. Hinde, D. Hilscher, H. Rossner, B. Gebauer, M. Lehmann, and M. Wilpert, Phys. Rev. C **45**, 1229 (1992).

[4] J. P. Lestone, Phys. Rev. Lett. **70**, 2245 (1993).

[5] J. U. Andersen, J. Chevallier, J. S. Forster, S. A. Karamian, C. R. Vane, J. R. Beene, A. Galindo-Uribarri, J. GomezdelCampo, H. F. Krause, E. Padilla-Rodal, D. Radford, C. Broude, F. Malaguti, and A. Uguzzoni, Phys. Rev. Lett. **99**, 162502 (2007).

[6] M. Morjean, A. Chbihi, C. Escano-Rodriguez, J. D. Frankland, C. Stodel, D. Jacquet, M. Laget, L. Tassan-Got, J. L. Charvet, R. Dayras, A. Drouart, L. Nalpas, C. Volant, A. LHoir, C. Cohen, M. Parlog, M. Chevallier, D. Dauvergne, R. Kirsch, P. Lautesse *et al.*, Phys. Rev. Lett. **101**, 072701 (2008).

[7] J. U. Andersen, J. Chevallier, J. S. Forster, S. A. Karamian, C. R. Vane, J. R. Beene, A. Galindo-Uribarri, J. G. del Campo, C. J. Gross, H. F. Krause, E. Padilla-Rodal, D. Radford, D. Shapira, C. Broude, F. Malaguti, and A. Uguzzoni, Phys. Rev. C **78**, 064609 (2008).

[8] H. W. Wilschut and V. L. Kravchuk, Nucl. Phys. A **734**, 156 (2004).

[9] M. O. Fregeau, D. Jacquet, M. Morjean, E. Bonnet, A. Chbihi, J. D. Frankland, M. F. Rivet, L. Tassan-Got, F. Dechery, A. Drouart, L. Nalpas, X. Ledoux, M. Parlog, C. Ciortea, D. Dumitriu, D. Fluerasu, M. Gugiu, F. Gramegna, V. L. Kravchuk, T. Marchi *et al.*, Phys. Rev. Lett. **108**, 122701 (2012).

[10] M. Morjean, J. L. Charvet, A. Chbihi, M. Chevallier, C. Cohen, D. Dauvergne, R. Dayras, A. Drouart, J. D. Frankland, D. Jacquet, R. Kirsch, M. Laget, P. Lautesse, A. L'Hoir, A. Marchix, L. Nalpas, M. Parlog, C. Ray, C. Schmitt, C. Stodel, L. Tassan-Got, and C. Volant, Eur. Phys. J. D **45**, 27 (2007).

[11] D. Jacquet and M. Morjean, Prog. Part. Nucl. Phys. **63**, 155 (2009).

[12] I. Gontchar, M. Morjean, and S. Basnary, Europhys. Lett. **57**, 355 (2002).

[13] M. T. Senthil Kannan, J. Sadhukhan, B. K. Agrawal, M. Balasubramaniam, and S. Pal, Phys. Rev. C **98**, 021601(R) (2018).

[14] N. K. Rai, A. Gandhi, M. T. Senthil Kannan, S. K. Roy, N. Saneesh, M. Kumar, G. Kaur, D. Arora, K. S. Golda, A. Jhingan, P. Sugathan, T. K. Ghosh, J. Sadhukhan, B. K. Nayak, N. K. Deb, S. Biswas, A. Chakraborty, A. Parihari, and A. Kumar, J. Phys. G: Nucl. Part. Phys. **49**, 035103 (2022).

[15] H. A. Kramers, Physica **7**, 284 (1940).

[16] N. Bohr and J. A. Wheeler, Phys. Rev. **56**, 426 (1939).

[17] D. J. Hinde, R. J. Charity, G. S. Foote, J. R. Leigh, J. O. Newton, S. Ogaza, and A. Chatterjee, Nucl. Phys. A **452**, 550 (1986).

[18] A. Saxena, A. Chatterjee, R. K. Choudhury, S. S. Kapoor, and D. M. Nadkarni, Phys. Rev. C **49**, 932 (1994).

[19] K. Mahata and S. Kailas, Phys. Rev. C **95**, 054616 (2017).

[20] T. Banerjee, S. Nath, and S. Pal, Phys. Rev. C **99**, 024610 (2019).

[21] V. Singh, B. Behera, M. Kaur, A. Jhingan, R. Kaur, P. Sugathan, D. Siwal, S. Goyal, K. P. Singh, S. Pal, A. Saxena, and S. Kailas, J. Phys. G: Nucl. Part. Phys. **48**, 075104 (2021).

[22] G. Chaudhuri and S. Pal, Phys. Rev. C **65**, 054612 (2002).

[23] K. Hagino, N. Rowley, and A. T. Kruppa, Comput. Phys. Commun. **123**, 143 (1999).

[24] P. Fröbrich and I. I. Gontchar, Phys. Rep. **292**, 131 (1998).

[25] J. Sadhukhan and S. Pal, Phys. Rev. C **78**, 011603(R) (2008); **79**, 019901(E) (2009).

[26] J. P. Lestone and S. G. McCalla, Phys. Rev. C **79**, 044611 (2009).

[27] J. P. Lestone, Phys. Rev. C **59**, 1540 (1999).

[28] A. V. Ignatyuk, G. N. Smirenkin, and A. S. Tishin, Sov. J. Nucl. Phys. **21**, 255 (1975).

[29] W. Reisdorf, Z. Phys. A **300**, 227 (1981).

[30] A. J. Sierk, Phys. Rev. C **33**, 2039 (1986).

[31] W. D. Myers and W. J. Swiatecki, Nucl. Phys. **81**, 1 (1966).

[32] S. Bjørnholm, A. Bohr, and B. R. Mottelson, in *Proceedings of the International Conference on the Physics and Chemistry of Fission*, Rochester, 1973 (IAEA, Vienna, 1974), Vol. 1, p. 367.

[33] A. V. Ignatyuk, G. N. Smirenkin, M. G. Itkis, S. I. Mul'gin, and V. N. Okolovich, Fiz. Elem. Chastits At. Yadra **16**, 709 (1985); Sov. J. Part. Nucl. **16**, 307 (1985).

[34] V. I. Zagrebaev, Y. Aritomo, M. G. Itkis, Y. T. Oganessian, and M. Ohta, Phys. Rev. C **65**, 014607 (2001).

[35] A. R. Junghans, M. de Jong, H.-G. Clerc, A. V. Ignatyuk, G. A. Kudyaev, and K.-H. Schmidt, Nucl. Phys. A **629**, 635 (1998).

[36] P. Grange, Li Jun-Qing, and H. A. Weidenmüller, Phys. Rev. C **27**, 2063 (1983).

[37] K. H. Bhatt, P. Grange, and B. Hiller, Phys. Rev. C **33**, 954 (1986).

[38] H. Hofmann and J. R. Nix, Phys. Lett. B **122**, 117 (1983).

[39] T. Banerjee, S. Nath, and S. Pal, Phys. Lett. B **776**, 163 (2018).

[40] A. Shrivastava, S. Kailas, A. Chatterjee, A. Navin, A. M. Samant, P. Singh, S. Santra, K. Mahata, B. S. Tomar, and G. Pollarolo, Phys. Rev. C **63**, 054602 (2001).

[41] E. Prasad, K. M. Varier, N. Madhavan, S. Nath, J. Gehlot, S. Kalkal, J. Sadhukhan, G. Mohanto, P. Sugathan, A. Jhingan, B. R.S. Babu, T. Varughese, K. S. Golda, B. P. AjithKumar, B. Satheesh, S. Pal, R. Singh, A. K. Sinha, and S. Kailas, Phys. Rev. C **84**, 064606 (2011).

[42] P. V. Laveen, E. Prasad, N. Madhavan, S. Pal, J. Sadhukhan, S. Nath, J. Gehlot, A. Jhingan, K. M. Varier, R. G. Thomas, A. M. Vinodkumar, A. Shamlath, T. Varughese, P. Sugathan, B. R. S.

Babu, S. Appannababu, K. S. Golda, B. R. Behera, V. Singh, R. Sandal, A. Saxena, B. V. John, and S. Kailas, J. Phys. G: Nucl. Part. Phys. **42**, 095105 (2015).

[43] E. Prasad, K. M. Varier, R. G. Thomas, K. Mahata, A. M. Vinodkumar, S. Appannababu, P. Sugathan, K. S. Golda, B. R. S. Babu, A. Saxena, B. V. John, and S. Kailas, *Proceedings of the DAE Symposium on Nucl. Phys.*, Pilani, 2010 (Board of Research in Nuclear Sciences, India), Vol.55, p.310.

[44] A. C. Berriman, D. J. Hinde, M. Dasgupta, C. R. Morton, R. D. Butt, and J. O. Newton, Nature (London) **413**, 144 (2001).

[45] H. Hofmann, Phys. Rep. **284**, 137 (1997).

[46] K. S. Golda, A. Saxena, V. K. Mittal, K. Mahata, P. Sugathan, A. Jhingan, V. Singh, R. Sandal, S. Goyal, J. Gehlot, A. Dhal, B. R. Behera, R. K. Bhowmik, and S. Kailas, Nucl. Phys. A **913**, 157 (2013).

[47] K. Mazurek, P. N. Nadtochy, E. G. Ryabov, and G. D. Adeev, Eur. Phys. J. A **53**, 79 (2017).

[48] M. D. Usang, F. A. Ivanyuk, C. Ishizuka, and S. Chiba, Phys. Rev. C **94**, 044602 (2016).

[49] T. Mukhopadhyay and S. Pal, Phys. Rev. C **56**, 296 (1997).

[50] R. J. Charity, arXiv:nucl-th/0406040.

[51] R. Sandal, B. R. Behera, V. Singh, M. Kaur, A. Kumar, G. Singh, K. P. Singh, P. Sugathan, A. Jhingan, K. S. Golda, M. B. Chatterjee, R. K. Bhowmik, S. Kalkal, D. Siwal, S. Goyal, S. Mandal, E. Prasad, K. Mahata, A. Saxena, J. Sadhukhan, and S. Pal, Phys. Rev. C **87**, 014604 (2013).

[52] H. Singh, K. S. Golda, S. Pal, Ranjeet, R. Sandal, B. R. Behera, G. Singh, A. Jhingan, R. P. Singh, P. Sugathan, M. B. Chatterjee, S. K. Datta, A. Kumar, G. Viesti, and I. M. Govil, Phys. Rev. C **78**, 024609 (2008).

[53] N. Kumar, S. Verma, S. Mohsina, J. Sadhukhan, K. Rojeeta Devi, A. Banerjee, N. Saneesh, M. Kumar, R. Mahajan, M. Thakur, G. Kaur, A. R. Neelam, A. Yadav, K. R. Kumar, U. S. Mandal, S. Kumar, B. R. Behera, K. S. Golda, A. Jhingan, and P. Sugathan, Phys. Lett. B **814**, 136062 (2021).

[54] P. N. Patil, N. M. Badiger, B. K. Nayak, S. Santra, P. C. Rout, A. Pal, G. Mohanto, K. Mahata, K. Ramachandran, R. G. Thomas, E. T. Mirgule, N. Madhavan, R. Gandhi, M. M. Hosamani, A. Vinayak, A. Kundu, S. De, S. P. Behera, B. Srinivasan, A. Saxena, and V. D. Bharud, Phys. Rev. C **102**, 034618 (2020).

[55] H. Eslamizadeh and H. Falinejad, Phys. Rev. C **105**, 044604 (2022).